Estimating Airflow Patterns Over Complex Terrain

Michael A. Fosberg, William E. Marlatt, and Lawrence Krupnak

USDA Forest Service
Research Paper RM-162
Rocky Mountain Forest and
Range Experiment Station
Forest Service
U.S. Department of Agriculture
Fort Collins, Colorado 80521

March 1976

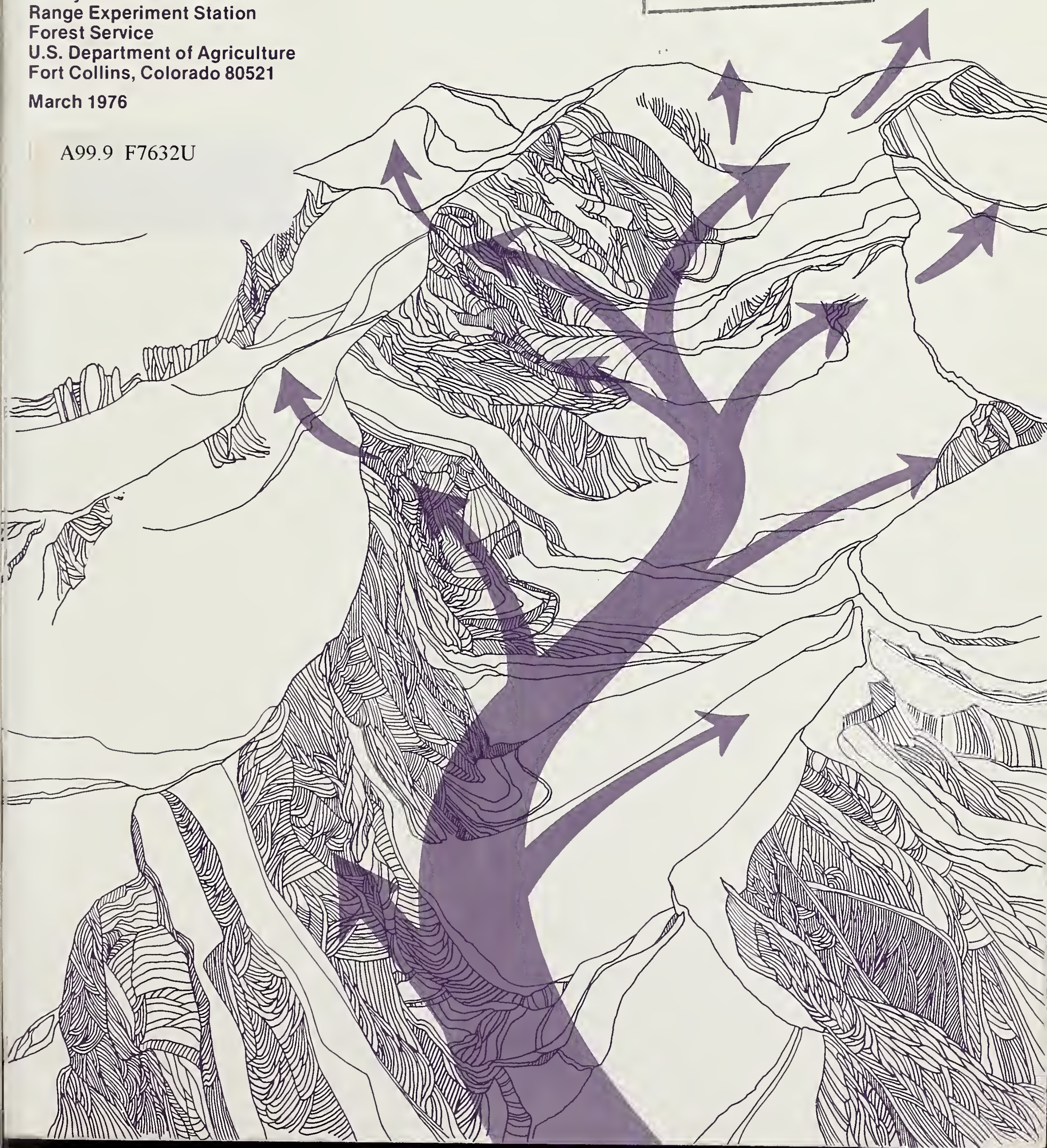

Abstract

Fosberg, Michael A., William E. Marlatt, and Lawrence Krupnak. 1976. Estimating airflow patterns over complex terrain. USDA For. Serv. Res. Pap. RM-162, 16 p. Rocky Mt. For. and Range Exp. Stn., Fort Collins, Colo. 80521.

A simple one-layer model of atmospheric boundary layer flow was developed for use in complex terrain. The model was derived through simplification of the fundamental Navier-Stokes flow equations. This simplification was gained by neglecting advection terms in the equations of motion and by assuming an impulse solution.

Although the equations do not describe all flow characteristics, the resultant solution describes a diagnostic model of the vector flow field. It requires much less data than traditional approaches, and therefore can be used as an estimator of wind patterns in areas where dense observational networks are not economically feasible.

The intended primary uses for this model are in providing wind fields for fire behavior prediction and in evaluation of pollution transport patterns.

Keywords: Wind, boundary layer, air pollution, fire weather.

USDA Forest Service
Research Paper RM-162

March 1976

Estimating Airflow Patterns Over Complex Terrain

Michael A. Fosberg,[1] William E. Marlatt,[2] and Lawrence Krupnak[3]

[1]*Principal Meteorologist, Rocky Mountain Forest and Range Experiment Station, with central headquarters maintained at Fort Collins, Colorado, in cooperation with Colorado State University.*

[2]*Professor, Department of Earth Resources, Colorado State University, Fort Collins, Colorado.*

[3]*Graduate Research Assistant, Department of Earth Resources, Colorado State University, Fort Collins, Colorado.*

Contents

Estimating Airflow Patterns Over Complex Terrain

Michael A. Fosberg, William E. Marlatt, and Lawrence Krupnak

Introduction

Land managers are increasingly faced with problems requiring quantitative estimates of airflow patterns over complex terrain. Use of the wind information may range from potential air quality analysis for land use planning to predicting spread of actual wildfires. Areas in which such analysis is required are typically mountainous. Nearly always, evaluation is severely hampered by a single problem—lack of data, particularly wind data.

For these reasons, a method of determining boundary layer flow patterns is needed as an alternative to expensive data networks.

Boundary layer flow over complex terrain cannot currently be numerically modeled with complete fluid and thermodynamic equations. Accuracy and quantity of the initial data fields required for complete solution only shift the problem back to need for expensive data networks (Fosberg 1967, 1969). While these costs and efforts may be worthwhile in special locations and for specific problems, flexibility in geographic location and timeliness of solutions are sacrificed. We feel that an alternative procedure is required for wind pattern analysis which provides geographic flexibility and does not require sophisticated, expensive data networks. Such solutions cannot include all atmospheric processes, however. The governing equations must be simplified and some important effects must be represented by parameterized analogs.

A model of this type is based on tradeoffs between simplified solutions and preservation of realistic results. Several models of thermal and terrain-induced perturbation of near-ground flow have been developed recently. Anderson (1971) and Lantz[4] developed single layer models of two-dimensional potential flow over terrain features. Anderson (1971), Fosberg et al. (1972), and Fosberg[5] examined the thermally driven flow disturbances. These studies were all based on the philosophical argument that major simplification of the equations was acceptable, and that the disturbed flow field could be superimposed on a mean flow field. While superficially attractive, these preliminary models did not evaluate the consequences of the simplifications, nor did they provide quantitative arguments supporting neglect of specific processes.

Each of the models describes a single layer of finite depth, depicts a quasi-horizontal slab, and treats body forces as an impulse acceleration. The models also require the flow to be statically stable, either as an incompressible fluid or through the hydrostatic assumption. Superposition of disturbed flows on the mean flow also implies limitations on the processes that can be modeled. Impulse accelerations tacitly imply that a model is intended as a diagnostic tool rather than a time-dependent predictive model. Also, these models generally neglect or highly linearize the advection terms in the dynamic equations.

The highly idealized treatment of the advection term is probably the most serious of the assumptions. Justification is provided partially by examination of the energy integrals in Fos-

[4]Lantz, R. B. 1972. Application of a three dimensional numerical model to air pollution calculations. Preprint of paper presented at 65th Annu. Meet., Air Pollution Control Assoc., Miami Beach, Fla., June 18-22, 22 p.

[5]Fosberg, Michael A. (in press). New technology for determining atmospheric influence on smoke concentrations. Proc. Int. Symp. on Air Quality and Smoke from Urban and For. Fires, 1973. 11 p.

berg's (1967, 1969) analysis of flow over single ridges. Conversion of potential energy to kinetic energy dominates the kinetic energy budget. The advective redistribution of kinetic energy and the viscous dissipation are about an order of magnitude smaller. While these energy budget comparisons do not fully justify neglect of the advective processes, they do show that the assumption does not invalidate the models, but only restricts interpretation of the results.

In general, this class of airflow models excludes the small-scale physical situations in which transient or highly interactive processes such as gravity waves or unstable thermal convection dominate the flow field. Also, because of the restrictions imposed on the advection terms, downwind wake effects are not properly represented.

Use of these simplified models—rather than complex and complete solutions or as a substitute for extensive field studies—becomes attractive when extensive data are not available, or in land use planning where alternatives may be great, the time span for planning short, and the accuracy or costs of more physically precise solutions and studies unwarranted.

The model described in this paper is intended to meet these applied objectives. This model is based on simplified solutions of the complete equations. It is philosophically identical to the preliminary models, but combines more of the physical processes.

Structure of the Model

The mathematical model is based on the terrain-induced flow processes derived by Anderson (1971) and the thermally induced flows described by Fosberg et al. (1972). In addition, the frictional terms are included in the model. Anderson's model was based only on a form of the divergence equation, while the Fosberg et al. (1972) model was based only on the vorticity equation. The model developed here is developed from both equations.

The advection terms were neglected in both previous equations. The consequences of this assumption are that the equations were simplified at the expense of losing a complete physical description of the dynamic processes. Thermally, frictionally and terrain-induced flows were superimposed on a background potential flow across the computational boundaries. Each of these disturbances was assumed to take place only within the computational area. Superposition of disturbances on the background flow, after neglecting advection terms, is physically analagous to an impulse acceleration. The diagnostic nature of the model was achieved by allowing the impulse to act over a small, finite time interval defined by phase velocities of disturbances. Flow following the ground surface was obtained by a coordinate transform. A rigid upper surface above the terrain was assumed in order to define the top of the atmospheric slab.

Procedures for solving the equations involve serial approximations which superimpose a new physical effect on the previous solution. The first step in the solution was to transfer the large-scale background wind into a terrain-induced modification of the throughflow. This step provided a local throughflow wind.

Next, thermal and frictional modification of the vorticity and divergence were introduced. These changes were superimposed on the terrain-induced flow. Finally, stream functions and velocity potentials were calculated so that the windspeed and direction could be defined at all interior points.

Throughflow Representation

Total airflow through the computation field was required to satisfy conservation of mass. Since the lower surface of the layer was mountainous, provisions had to be made for local channeling and deflection. Throughflow characteristics were calculated from the steady-state mass continuity equation as outlined by Anderson (1971). Vertical integration and use of the anelastic approximation permitted local velocities to be approximated from the overall wind field and terrain features. The steady-state continuity equation is:[6]

$$\nabla \cdot \rho \underset{\sim}{v} = - \frac{\partial(\rho w)}{\partial z}$$

In this equation, ∇ is the horizontal gradient operator, ρ is density, $\underset{\sim}{v}$ is the velocity vector, and w is the vertical motion, positive upward.

Vector coordinates used in the mathematics are west to east in the x direction, south to north in the y direction, and vertically as z.

The anelastic approximation, where kinematic influences on density are negligible compared to thermodynamic influences, was first applied to the equation:

$$\bar{\rho}\, \nabla \cdot \underset{\sim}{v} = - \frac{\partial(\rho w)}{\partial z}$$

[6]*See appendix for a complete description of notations used in the equations.*

Bars over a variable indicate a mean value for the slab. The equation was then integrated over the depth of the layer between the ground (h) and the top of the slab (H).

$$\bar{\rho}\int_h^H \nabla\cdot\underset{\sim}{v}\, dz = -\int_h^H \frac{\partial(\rho w)}{\partial z}$$

Horizontal divergence was defined as $\delta = \nabla \cdot \underset{\sim}{v}$ so that the integral equation was solved as:

$$\bar{\rho}\,\bar{\delta}\,(H-h) = -\rho w(H) + \rho w(h)$$

through the mean value theorem. A rigid lid was assumed, so $\rho w(H)$ became zero. Vertical motion near the ground was assumed to be dominated by orographic lifting. The horizontal divergence of the mean wind field then became:

$$\bar{\delta} = \frac{\rho}{\bar{\rho}}\,\underset{\sim}{v}\cdot\frac{\nabla h}{(H - h)} \tag{1}$$

Terrain modification of the large-scale flow could then be calculated from the channeling and deflection of this flow, and could provide a first approximation of the local wind.

Thermal and Frictional Influences

Modification of the wind field produced by thermal acceleration and retardation required invoking the assumptions associated with the advection terms of the complete equations. Frictional influences were included as spatial variations of idealized and parameterized solutions relating surface characteristics to the wind profile. The fundamental procedure was to: (1) derive the complete divergence and vorticity equations, (2) judiciously neglect the advective terms, (3) allow full influence of the thermal terms, and (4) utilize classic frictional solutions.

The procedure required for inclusion of these body forces was to define the thermal and frictional solutions in terms of the Navier-Stokes equations. The first step was to express the divergence equation utilizing these assumptions. Divergence was obtained through:

$$\nabla\cdot\frac{d\underset{\sim}{v}}{dt} = \frac{\partial\delta}{\partial t} = \nabla\cdot(-c_p\Theta\nabla p_*) + \nabla\cdot(K\nabla^2\underset{\sim}{v})$$

where θ is the potential temperature, p_* is the pressure variable defined as $p_* = T/\theta$, and K is the turbulent viscosity. The friction term was simplified to:

$$\nabla\cdot K\left(\frac{\partial^2\underset{\sim}{v}}{\partial z^2}\right) = K\left(\frac{\partial^3 u}{\partial x\partial z^2} + \frac{\partial^3 v}{\partial y\partial z^2}\right)$$

since the horizontal dissipation terms are small compared to the vertical terms when expressed in finite-difference mesoscale models. A parameterized form of the dissipation was obtained from the logarithmic wind profile near the ground. The wind profile for an adiabatic surface layer (Sutton 1953) is:

$$\frac{\partial u}{\partial z} = \frac{u_*}{kZ^2} \text{ and } \frac{\partial v}{\partial z} = \frac{v_*}{kZ^2} \tag{2}$$

where u_* and v_* are the friction velocities and k is the von Karman constant. These two functions were differentiated with respect to z to produce the second derivative. The terms

$$\frac{\partial^2 u}{\partial z^2} = -\frac{u_*}{kZ^2} \text{ and } \frac{\partial^2 v}{\partial z^2} = -\frac{v_*}{kZ^2}$$

were then substituted into the divergence equation. The divergence equation then became:

$$\frac{\partial\delta}{\partial t} = -c_p\Theta\nabla^2 p_* - c_p\nabla\Theta\cdot\nabla p_* - \frac{K}{kZ^2}\left(\frac{\partial u_*}{\partial x} + \frac{\partial v_*}{\partial y}\right) \tag{3}$$

Friction velocity was obtained by integrating the wind profile equation for fully rough surfaces. The friction velocities are then:

$$u_* = \frac{|\bar{u}|k}{\ln\left(\frac{Z + z_o}{z_o}\right)} \tag{4a}$$

$$v_* = \frac{|\bar{v}|k}{\ln\left(\frac{Z + z_o}{z_o}\right)} \tag{4b}$$

where z_o is the surface roughness length and Z is the height of the wind above ground.

Rotational flow characteristics were introduced through the vorticity equation. Using the same assumptions for this derivation as were

used in the development of the divergence equation, the vorticity equation became:

$$k \cdot \nabla x \frac{d\tilde{v}}{dt} = \frac{\partial \zeta}{\partial t} = -c_p \frac{\partial(\Theta, p_*)}{\partial(x, y)} - (\zeta + f)\,\delta - \frac{K}{kZ^2}\left(\frac{\partial v_*}{\partial x} - \frac{\partial u_*}{\partial y}\right) \tag{5}$$

The divergence and vorticity equations are time-dependent and therefore must be integrated. Divergence was integrated directly through the mean value theorem over an arbitrary time interval. Since little is known about the rate of change of divergence, a square wave impulse of interval Δt_δ was assumed. The integrating time factor then became $\frac{1}{2}\Delta t_\delta$ when the magnitude of the acceleration was assumed to be ½ the observed or maximum value. Divergence was then:

$$\partial = \tfrac{1}{2}\Delta t\delta \left[-c_p \Theta \nabla^2 p_* - c_p \nabla\Theta \cdot \nabla p_* - \frac{K}{kZ^2}\left(\frac{\partial u_*}{\partial x} + \frac{\partial v_*}{\partial y}\right)\right] + \bar{\delta} \tag{6}$$

Given this solution, the vorticity equation became the ordinary differential equation of:

$$\frac{\partial \zeta}{\partial t} + \zeta\delta = -c_p \frac{\partial(\Theta, p_*)}{\partial(x,y)} - f\delta - \frac{K}{kZ^2}\left(\frac{\partial v_*}{\partial x} + \frac{\partial u_*}{\partial y}\right)$$

The solution is:

$$\zeta = e^{-\int \delta dt} \int \left[-c_p \frac{\partial(\Theta, p_*)}{\partial(x,y)} - f\delta - \frac{K}{kZ^2}\left(\frac{\partial v_*}{\partial x} - \frac{\partial u_*}{\partial y}\right)\right] \exp\left(\int \delta dt\right) dt + ce^{-\int \delta dt}$$

Again, an impulse of finite time interval Δt_ζ was assumed, so that the mean value integration gave:

$$\zeta = \exp(-\tfrac{1}{2}\delta\Delta t_\zeta)\ \tfrac{1}{2}\Delta t_\zeta \left[-c_p \frac{\partial(\Theta, p_*)}{\partial(x,y)} - f\delta - \frac{K}{kZ^2}\left(\frac{\partial v_*}{\partial x} - \frac{\partial u_*}{\partial y}\right)\right] \exp(\tfrac{1}{2}\delta\Delta t_\zeta) + ce^{-\delta\Delta t_\zeta/2}$$

The arbitrary time intervals for the divergence and vorticity were defined in terms of phase velocities. Because a rigid lid was used as an upper boundary for the calculation and an anelastic approximation was used for compressibility, the phase velocity for divergence was taken as the speed of sound. This gave a time interval of:

$$\Delta t_\delta = \frac{\text{sec}\ \Delta}{300\ \text{m}}$$

where Δ is the minimum distance between computational points. Phase velocities for vorticity were taken to be the large-scale windspeed, so that the time interval for vorticity was:

$$\Delta t_\zeta = \frac{\Delta}{(u^2 + v^2)^{\frac{1}{2}}}$$

For typical distances of 1 to 10 km between computational points and windspeeds of 1 to 10 m per second, the time interval is of the order of 1,000 seconds. Divergence at the mesoscale is typically 10^{-5} to 10^{-3} per second. These magnitudes suggested the exponential term in the vorticity equation should be approximately one, except under condition of light winds and large grid spacing. The constant of integration was then taken to be the large-scale flow vorticity. The vorticity then became:

$$\zeta = \tfrac{1}{2}\Delta t_\zeta \left[-c_p \frac{\partial(\Theta, p_*)}{\partial(x,y)} - f\delta - \frac{K}{kZ^2}\left(\frac{\partial v_*}{\partial x} - \frac{\partial u_*}{\partial y}\right)\right] + \zeta_0 \tag{7}$$

Equations (1) and (6) for the frictionally, thermally and terrain-induced flow deviations on divergence, and equation (7) for the frictionally and thermally induced flow deviations on rotation, were then used to calculate the wind components.

Calculation of Local Winds

Wind components of the flow were calculated in the area by superimposing the terrain, frictional, and thermal deviations on the large-scale wind. The wind deviations were obtained by separating the flow into an irrotational divergent component and a nondivergent rotational component. The divergent flow was described with a velocity potential and the rotational component with a stream function. The deviation velocity was then:

$$\underset{\sim}{v} = \underset{\sim}{k} x \nabla \psi + \nabla \phi$$

where ψ is the stream function and ϕ is the velocity potential. The vorticity is:

$$\zeta = k \cdot \nabla x \underset{\sim}{v} = \underset{\sim}{k} \cdot \nabla x \underset{\sim}{k} x \nabla \psi + \underset{\sim}{k} \cdot \nabla x \nabla \phi = \nabla^2 \psi \quad (8)$$

and the divergence is:

$$\delta = \nabla \cdot \underset{\sim}{v} = \nabla \cdot \underset{\sim}{k} x \nabla \psi + \nabla \cdot \nabla \phi = \nabla^2 \phi \quad (9)$$

Since the vorticity and divergence were known from equations (1), (6), and (7), the stream function and velocity potential could be obtained from a numerical solution of the elliptical differential equations (8) and (9). Decomposing the velocity into the west-east component and the south-north component, and superimposing the background flow, the velocities are:

$$u = u_o + \frac{\partial \phi}{\partial x} - \frac{\partial \psi}{\partial y} \quad (10a)$$

and

$$v = v_o + \frac{\partial \phi}{\partial y} + \frac{\partial \psi}{\partial x} \quad (10b)$$

where u_o and v_o are the background velocities.

Flow Near the Ground Surface

Airflow along the terrain surface is of much more interest in fire or air-quality studies than flow at some fixed elevation. Since the equations require calculations to be made on a flat horizontal surface, transformations from the horizontal plane to the terrain surface are necessary.

Data required by the model are observed at a fixed height above the ground (generally between 1 and 3 m) so the transforms chosen were to restructure the observed data to a flat surface locally, and then to consider the model as being composed of a series of adjacent horizontal surfaces, each of slightly different elevation based on the elevation of the local terrain. The coordinate transform required expressing the derivations of the variables observed on the terrain surface as though they were along a horizontal surface. If vertical variations of the variables are known, the transform for any quantity, S, is then:

$$\left.\frac{\partial S}{\partial x}\right)_E = \left.\frac{\partial S}{\partial x}\right)_T - \left.\frac{\partial S}{\partial z}\frac{\partial h}{\partial x}\right)_T$$

where the unsatisfied parentheses indicate derivations taken along either constant elevation or along the terrain surface.

Second derivations were obtained similarly as:

$$\left.\frac{\partial^2 S}{\partial x^2}\right)_E = -2\frac{\partial^2 S}{\partial x \, \partial z}\frac{\partial h}{\partial z} - \frac{\partial S}{\partial z}\frac{\partial^2 h}{\partial x^2} + \left(\frac{\partial h}{\partial x}\right)^2 \frac{\partial^2 S}{\partial_z 2}$$

The higher order terms involving derivatives of the terrain are small compared to the linear term. Six separate derivatives of the thermal characteristics are required by the vorticity and divergence equations. These are the first derivative of potential temperature and pressure, and the second derivative of pressure in the cardinal directions.

Vertical variations of these thermodynamic variables are required. These were obtained first for potential temperature through static stability for a hydrostatically balanced atmosphere as:

$$\left.\frac{\partial \Theta}{\partial x}\right)_E = \left.\frac{\partial \Theta}{\partial x}\right)_T - \Theta\sigma \left.\frac{\partial h}{\partial x}\right)_T \quad (11a)$$

$$\left.\frac{\partial \Theta}{\partial y}\right)_E = \left.\frac{\partial \Theta}{\partial y}\right)_T - \Theta\sigma \left.\frac{\partial h}{\partial y}\right)_T \quad (11b)$$

where $\sigma = \frac{1}{\theta} \frac{\partial \theta}{\partial z}$.

Vertical decrease of pressure was represented by hydrostatic equilibrium:

$$\frac{\partial p_*}{\partial z} = - \frac{g}{c_p \Theta}$$

Utilizing these relationships, the pressure derivatives are:

$$\left.\frac{\partial p_*}{\partial x}\right)_E = \left.\frac{\partial p_*}{\partial x}\right)_T + \left.\frac{g}{c_p\Theta}\frac{\partial h}{\partial x}\right)_T \tag{11c}$$

$$\left.\frac{\partial p_*}{\partial y}\right)_E = \left.\frac{\partial p_*}{\partial y}\right)_T + \left.\frac{g}{c_p\Theta}\frac{\partial h}{\partial x}\right)_T \tag{11d}$$

$$\left.\frac{\partial^2 p_*}{\partial x^2}\right)_E = \left.\frac{\partial^2 p_*}{\partial x^2}\right)_T - 2\left.\frac{g}{c_p\Theta^2}\frac{\partial h}{\partial x}\frac{\partial\Theta}{\partial x}\right)_T \tag{11e}$$

$$\left.\frac{\partial^2 p_*}{\partial y^2}\right)_E = \left.\frac{\partial^2 p_*}{\partial y^2}\right)_T - 2\left.\frac{g}{c_p\Theta^2}\frac{\partial h}{\partial y}\frac{\partial\Theta}{\partial y}\right)_T \tag{11f}$$

Horizontal derivatives of the friction velocities remain unchanged, since the model is designed for use in the constant flux layer where they are constant in the vertical. This shallow layer assumption then gives:

$$\left.\frac{\partial u_*}{\partial x}\right)_E = \left.\frac{\partial u_*}{\partial x}\right)_T \tag{11g}$$

$$\left.\frac{\partial u_*}{\partial y}\right)_E = \left.\frac{\partial u_*}{\partial y}\right)_T \tag{11h}$$

$$\left.\frac{\partial v_*}{\partial x}\right)_E = \left.\frac{\partial v_*}{\partial x}\right)_T \tag{11i}$$

$$\left.\frac{\partial v_*}{\partial y}\right)_E = \left.\frac{\partial v_*}{\partial y}\right)_T \tag{11j}$$

These linear coordinate transforms neglect the small changes in the grid spacing due to slope distances projected to the horizontal grid.

Data Requirements and Solution Procedure

Specific data required by the model are temperature, pressure, elevation, and roughness length of the underlying surface for all computational points. Temperature and pressure data are transformed thermodynamically to model variables by:

$$\Theta = \frac{T}{p_*} \tag{12}$$

and

$$p_* = \left(\frac{p}{p_o}\right)^{\frac{R}{c_p}} = \left(\frac{p}{p_o}\right)^{0.2857} \tag{13}$$

where p_0 is a reference pressure and T is expressed in an absolute temperature scale. While any consistent set of units may be used, the appendix list of symbols gives constants only in metric units.

Roughness lengths are a reasonably constant value describing the height at which the mean wind flow is zero. These values are conveniently describable to acceptable accuracy by classifying the surface into such categories as (but not limited to) grass, brush, boulder field, and so forth. These data are tabulated in numerous texts (Sutton 1953, Priestley 1959, and Sellers 1965); a sample listing is provided in table 1 for convenience and completeness.

Table 1.--Relationship between surface roughness and surface features

Classification of underlying surface	Typical value of roughness length (z_o)	
	cm	
Mud flats, ice	0.001	(Sutton 1953)
Smooth snow	0.005	(Priestley 1959)
Snow, prairie	0.01	"
Thin grass up to 50 cm high	5	(Sutton 1953)
Thick grass up to 50 cm high	9	"
Wheat	22	(Sellers 1965)
City	165	"
Orchard	198	"
Fir forest	283	"

Since the model was designed for use in moderately small areas of finite size, several single-valued coefficients are required to complete the model. Most important of these are the static stability and the large-scale wind direction and windspeed. The large-scale winds were specified as the geostrophic wind. Less important coefficients are the eddy viscosity, the latitude (if the geographic scale of a particular solution is large so that the earth's rotation is important), and the large-scale vorticity (if strong curvature exists in the large-scale flow).

Wind patterns are calculated from a sequence of approximations, each refining the previous step by introducing a more refined physical process, and superimposing the refinement on the previous solution. The first step was to transfer the large-scale background wind into a major terrain-induced modification of the throughflow. This step provided a local throughflow wind.

First, the divergence was calculated through equation (1) for a smoothed terrain. This smoothed terrain was obtained by averaging the four surrounding points with each computational point; the rigid lid was placed well above the terrain in this step. Second, the terrain-induced vorticity was calculated by equation (7) with the thermal and frictional terms neglected. Once these vorticities and divergences were calculated, they were transformed to stream functions and velocity potentials through numerical solutions of equations (8) and (9), and subsequently resolved into velocities by equation (10). These first approximations to the wind field represented the influences of the large terrain feature on the throughflow.

The second level of approximation involved recalculating the terrain-induced divergence for a shallow layer. Divergence was calculated by equation (1) for the actual terrain.

The next step required using the large-scale terrain flow to calculate the friction velocities by equations (4a and 4b) and making the coordinate transforms of equation (11). These intermediate steps provided the input to the final level of approximation.

Friction terms, defined by the friction velocity, and the spatial derivations of temperature and pressure after the coordinate transform were included in the solution of equation (6) for divergence and of equation (7) for vorticity. Background divergence came from the second level of approximation, and the background vorticity came from the divergence and vorticity as in the first step through numerical solutions of equations (8) and (9). Velocity components were then calculated through equation (10), where the background velocities were defined by the first step.

Evaluation of the Model

Validation

There are several philosophies of model validation, each designed to accomplish specific objectives. Because this model is intended for use in applied meteorology, we have chosen to use actual data sets from mountain mesoscale studies to validate the wind field estimates. In adopting this approach, we have imposed a severe test since the model is limited in spatial resolution by computational filtering to approximately four times the grid distance, while the validation data have small-scale spatial resolutions defined by nearby terrain or vegetation and sensor response characteristics. Also, calculated winds represent an average wind over an area defined by the grid mesh. Such a test is desirable, however, because it defines operational uncertainty rather than model potential, and represents actual resolution attainable.

Seven data sets were used in the model validation. Six came from studies conducted by Cramer[7] in the Oregon Cascade Mountains. One data set came from central California (Fosberg and Schroeder 1966). All seven depict daytime conditions: five for midafternoon, and two for morning. One morning case occurred under overcast skies and rain. The other six occurred with strong solar heating. Background winds ranged from 2 to 5 m per second. The Oregon winds were calculated on a 6 km square grid, the California case on a 16 km square grid. Air temperatures were extrapolated to grid points from the field network weather stations.

Evaluation of the errors in both windspeed (fig. 1) and wind direction (fig. 2) demonstrates the utility of the model. The root mean square windspeed error was 2.0 m per second. Forty-five percent of the calculated windspeeds fell within 1 m per second of the observed wind, and 75 percent fell within 2 m per second. These comparisons were made over an observed range of 0.5 to 10.5 m per second. Observed wind directions were reported on a 16-point compass basis. Therefore, the error analysis is presented as a compass-point error rather than a more precise evaluation

[7] *We thank Owen P. Cramer of the U.S. Department of Agriculture, Forest Service, Pacific Northwest Forest and Range Experiment Station, Portland, Oregon for unqualified use of original data for the model validation and for permission to reproduce unpublished results in this paper.*

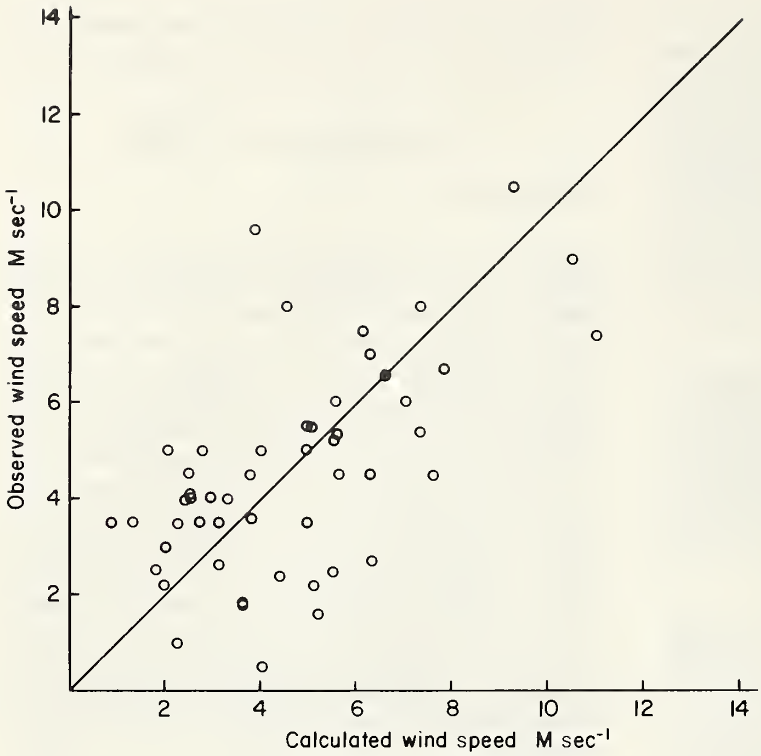

Figure 1.—Comparison of calculated and observed windspeeds. Bold diagonal line defines perfect fit. Forty-five percent of predictions tall within 1 m sec^{-1} of the observed windspeed and 75 percent fall within 2 m sec^{-1}.

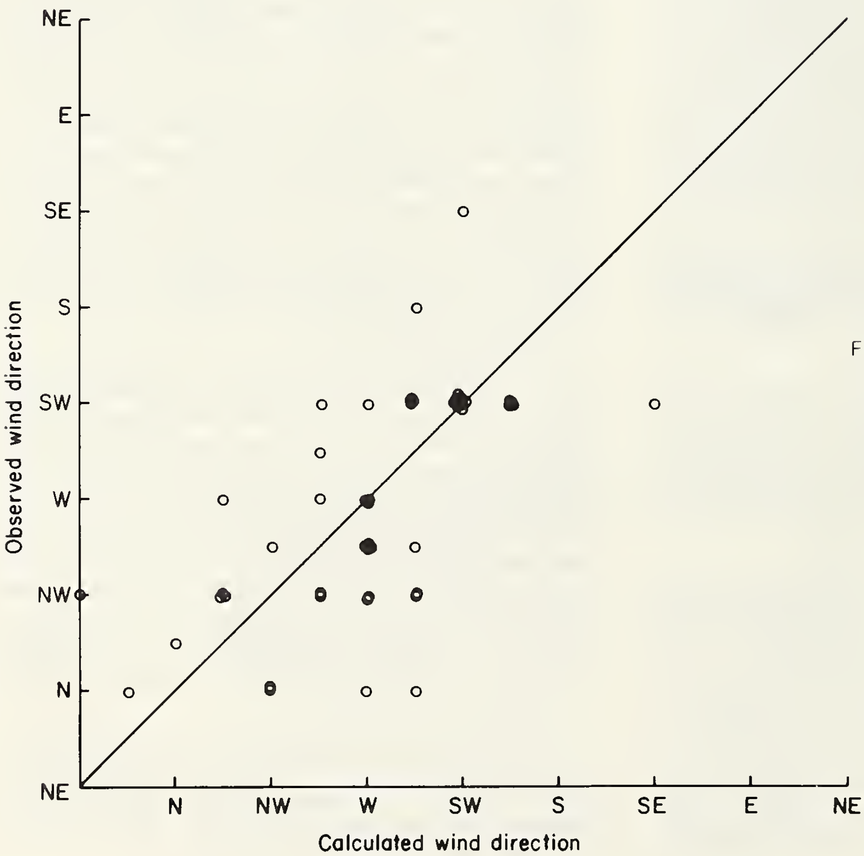

Figure 2.—Comparison of calculated and observed wind direction. Comparison is on a 16-point compass basis. Sixty percent of calculated directions tall within 11 degrees and 92 percent fall within 22 degrees of observed directions.

of angle. The root mean square direction error was 1.9 points. Sixty percent of the calculated directions fell within 1 compass point of the observed direction, and 92 percent fell within a 2-point envelope of the observed direction. Observed directions were from all compass points except for the east and northeast sections.

Models of this type implicitly require a number of specifiable coefficients which tune the model to particular geographic regions. While we have attempted to specify these coefficients through physical arguments, some are still at the discretion of the user. The integration coefficients were totally predetermined. The rigid lid coefficients for potential flow were selected through several criteria. The first was that the terrain could not penetrate the rigid lid. The second was based on a large number of solutions where the lid was systematically varied until a high level of sensitivity was reached. Lid height is based on elevation differences across the grid field. The user guidelines in the climatology section of this paper describe the techniques for determining layer thickness. They are cited here because the consequences are reflected in the error analysis.

Flow Patterns

Each of the seven cases showed similar dynamic processes (table 2). Thermally and terrain-produced divergence dominated the dynamics of the flow. Divergence-generated flow perturbations were 2.5 to 4.3 times as large as vortically generated deviations. Vortex flow accounted for 11 to 24 percent of total kinetic energy, while 32 to 69 percent was accounted for by the potential flow. Strongest local wind energetics were observed under conditions of light background winds and strong surface heating. As background winds increased, or the solar heating decreased, the local winds became a weaker component and less important in the total kinetic energy budget. Tests of background windspeeds for several hypothetical cases beyond the range of data used in validation show that at 0.5 m per second, the wind patterns are controlled completely by the thermal patterns. At 10 m per second, thermal control vanished and terrain influences were weak.

Mesoscale flow characteristics are best illustrated through a detailed examination of one of the case studies. The area is in the Oregon Cascades, south of Mt. Hood, north of Mt. Jefferson, and runs from the Willamette Valley across the crest of the Cascade Range to the edge of the eastern Oregon plateau. The mountains are penetrated by a major drainage on the west side, the Clackamas River. The particular case selected, August 8, 1963 at 1600 PST, was chosen as representing a typical or intermediate situation. The synoptic weather pattern was characterized by a weak upper-level, high-pressure area, and west to west-north-west geostrophic surface flow over the Cascades. Details of the observation and analysis procedures were presented in Cramer (1972) and Cramer and Lynott (1961, 1970). Discussion here is limited to resultant computations and estimation of the wind field from the analysis. Only salient features of Cramer's analysis are presented here for completeness.

Cramer's data analysis of temperature and 850 mb surface heights were interpolated to 6-km grid points. These data were converted to potential temperature and normalized station pressures for each grid point. Terrain elevation at each grid point was interpolated from a topographic map.

Table 2.--Relationship between flow energetics and weather features

Date	Location	Time	Flow energy accounted for by: Irrotational energy	Flow energy accounted for by: Rotational energy	Ratio of irrotational energy to rotational energy	Geostrophic windspeed	Weather features
		LST	*percent*	*percent*		*m per second*	
1963							
Aug. 8	Oregon	0700	60.4	24.3	2.5	2.5	Strong morning heating
Aug. 8		1600	55.1	19.8	2.8	2.5	Strong afternoon heating
Aug. 19		0700	34.2	9.1	3.8	4.9	Weak morning heating--extensive clouds and rain
Sept. 4		1600	31.5	10.7	2.9	4.9	Strong afternoon heating
Sept. 5		1600	42.7	15.7	2.7	3.5	Strong afternoon heating
Sept. 12		1300	68.5	20.7	3.3	2.5	Strong afternoon heating
1962							
Aug. 15	Calif.	1400	42.3	9.9	4.3	3.0	Strong afternoon heating

The underlying surface was almost exclusively characterized by conifer forest, so the roughness length was taken as a constant 283 cm.

Temperature distribution (fig. 3) over this terrain generally showed a slight decrease with elevation. West-facing slopes were warmer than east-facing slopes. The major river valley was much warmer than surrounding areas, and provided strong local temperature gradients. In general, the area east of the Cascades was warmest as a result of morning heating and topographic blocking of cool marine air flowing off the Pacific Ocean.

Height of the 850 mb pressure surface (fig. 4) generally reflected the high-pressure area over northwest Oregon. Surface heating of the mountain slopes produced the "thermal low" frequently observed along the West Coast. This "thermal low" appeared as a mesoscale low-pressure area through the higher terrain and modified the large-scale pressure pattern.

These observed data were transformed to the thermodynamic variables of potential temperature and normalized nondimensional surface pressure used in the model equations. The 850 mb surface height was reduced to the terrain surface through the hydrostatic equation using the static stability from the Salem, Oregon rawinsonde observation. Once this pressure calculation was made, the potential temperatures were calculated with these pressures and the interpolated temperatures.

Since the dynamic influences due to pressure gradients are completely reflected in the 850 mb pressure surface height, only the potential temperature patterns will be described here (fig. 5). Potential temperature showed a highly organized pattern. Higher elevations had higher potential temperatures. Valleys where cooler marine air could penetrate from the coast were clearly marked by low potential temperature. East-slope highlands had highest potential temperatures.

These observed fields of temperature and pressure were used to calculate the fundamental kinematic characteristics of divergence and vorticity. Divergence patterns were strongly correlated with terrain. Even small topographic features such as narrow ridges and valleys stand out in the divergence patterns (fig. 6). Flow divergence was confined to lowlands and valley bottoms. Convergence zones were on ridgetops and followed the terrain contours. Gentle slopes and large continuous upland areas on the east slopes typically had weak gradients. Magnitudes of the divergence were typically $\pm 10^{-3}$ per second. The convergence areas in regions of rugged terrain were much smaller than divergence areas, and maximum values were two to three times as intense as the compensating divergent areas. The intense gradients generated in the rugged terrain were most noticeable between the Clackamas River valley and the surrounding ridges. Areas of moderately changing terrain had divergent and convergent patterns of roughly equal area and intensity.

Vorticity patterns (fig. 7) did not show either the response to small terrain features or the large magnitude found in the divergence fields. Vorticity was typically $\pm 10^{-5}$ per second with the strongest areas only $\pm 10^{-4}$ per second. Ridgetops tended to have anticyclonic relative vorticity of 10^{-4} per second while valley bottoms had cyclonic vorticities of -10^{-4} per second. Areas with slowly changing elevation did not show a consistent terrain-vorticity correlation. In general, vorticity tended to have a much longer wave length than divergence. The only generalizations we can make about the patterns are that major ridges tend to favor anticyclonic vorticity, while lowlands and major valleys tend to favor cyclonic vorticity. This characteristic was probably due to the dominant influence of the divergence in flow properties.

Resultant wind fields (fig. 8) showed strong topographic and thermal control of the wind patterns. Airflow in the Clackamas River valley and the other two west-slope watersheds penetrating into the Cascades showed strong topographic channeling up the rivers and the influence of slope winds angling away from the valley axis. West-slope areas away from these major drainages generally showed upslope flow, even on the lee sides. Strongest winds were calculated on high ridgetops and at the heads of canyons as they reached the highlands. Lee effects were most noticeable along the eastern slope. Winds flowing across the ridge in the northeast portion of the area were reduced from 5 m per second to 1 m per second by the upslope influences on the lee side. Strong, thermally driven winds were calculated in the south-central and southeastern portion of the area, where prevailing winds were reduced and influences of the penetrating west-slope canyons were negligible. Those variables which had greatest impact on model reliability were determined by sensitivity analysis. Both processes and variables were systematically excluded and error analysis conducted on all seven cases. This analysis indicated that frictional influences and the vorticity equation affected the resultant wind field only slightly. Terrain and thermal influences totally dominated the calculations. Neglect of either created large errors in the wind field in the test cases. Further analysis of these processes indicated that pressure variation could be excluded with introduction of a small error, but that

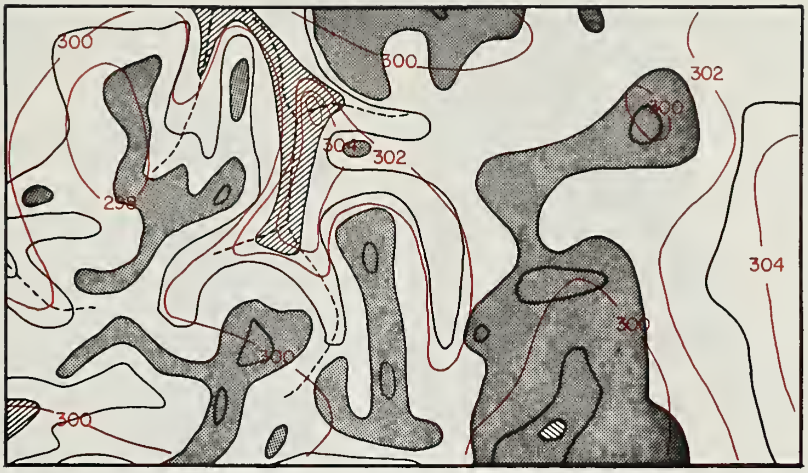

Figure 3.—Temperature field for 1600 PST, August 8, 1963. Temperatures are in degrees k; warmest areas are on the east slopes of the Cascade Mountains.

Figure 4.—Height of 850 mb surface for 1600 PST, August 8, 1963. Height is in meters above m.s.l. Thermal trough is oriented southwest to northeast.

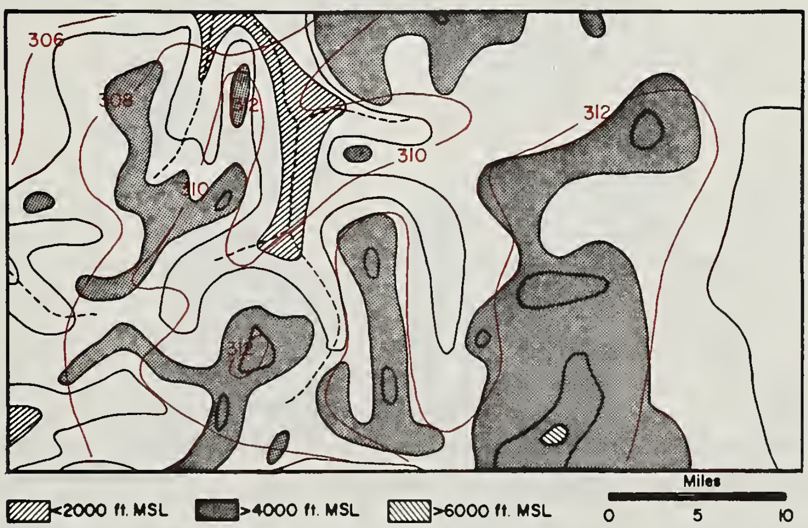

Figure 5.—Distribution of potential temperature for 1600 PST, August 8, 1963. Temperatures are in degrees k. Inversion of marine air into the mountains is confined to the Clackamas River valley.

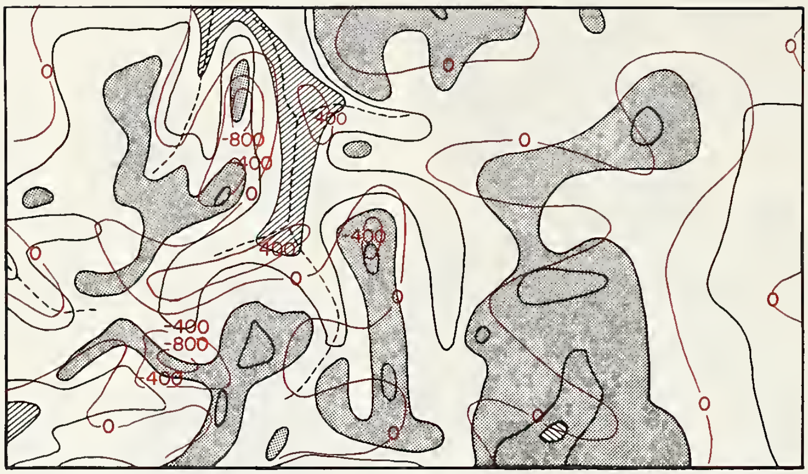

Figure 6.—Horizontal divergence field for 1600 PST, August 8, 1963. (Units are $10^{-5}sec^{-1}$.) Strongest gradients of divergence are between the west side drainages and the surrounding ridges.

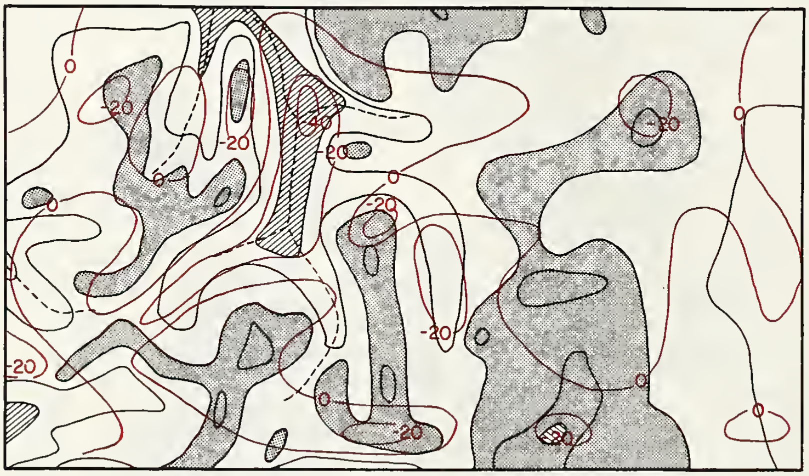

Figure 7.—Vertical component of vorticity for 1600 PST, August 8, 1963. (Units are $10^{-5}sec^{-1}$.) Anticyclonic vorticity is on ridgetops and cyclonic vorticity is in valleys.

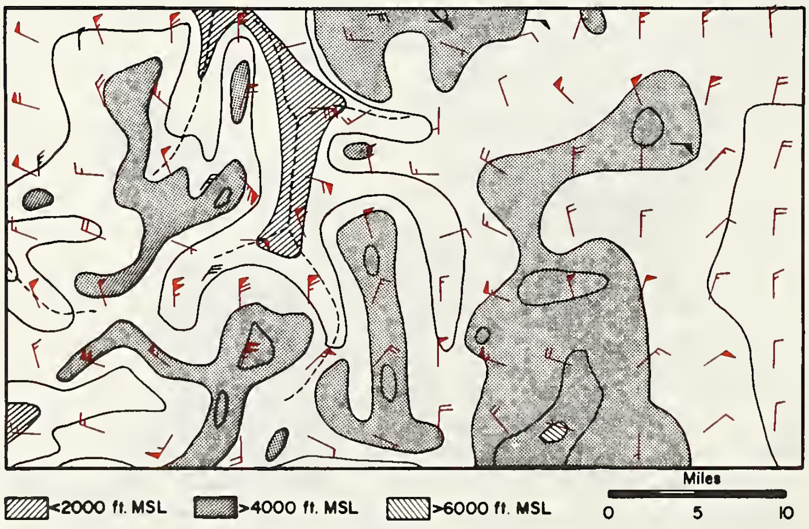

Figure 8.—Calculated and observed wind field for 1600 PST, August 8, 1963. Arrows indicate direction of wind. Speeds are given by sum of barbs and pennants on arrow tails. Pennants indicate 5 m sec^{-1}; a full barb, 2 m sec^{-1}; a half barb, 1 m sec^{-1}. Calculated wind field is in red; observed wind field is in black.

the topographic and temperature field must be represented in complete detail for the model to provide realistic and verifiable results.

Topography, Climatology, and Winds

Two parameters are required if the model is to define the topographic influence on throughflow. The first of these, the depth of the rigid lid at the top of the slab, should normally be expected to be 1,500 to 2,000 m above the spatially smoothed terrain. The second parameter, the thickness of the shallow layer, refines the first estimate of terrain influences. It is 1.25 times the difference between the smoothed terrain and the actual terrain. These guidelines for the relationship between throughflow and terrain were determined from a large number of test cases where the coefficients were varied systematically. The final choice was a judgment of which relationships produced the most acceptable resultant wind field.

Grid point spacing is also related to topographic variations. In rugged terrain, a closely spaced grid is required to resolve the local winds, while in gently rolling terrain, a low-resolution grid will give acceptable wind fields. Guidelines for selecting appropriate grid spacing were developed from procedures similar to those used in evaluating layer thicknesses.

Numerous analyses were carried out with the same data sets so that performance could be evaluated by overall resultant wind field errors. Grid spacings between 1 and 6 km were evaluated for maximum terrain differences of 300 to 1,500 m. These analyses indicated that grid spacing should be reduced by 1 km for every increase in terrain range of 300 m. If the terrain within an area 10,000 km square varies by 300 m or less between the highest and lowest spatially averaged elevations, then a 6-km grid would be appropriate. If, on the other hand, the terrain variation were 1,500 m a 1-km grid would be appropriate. These spacings must be modified to the smallest grid spacing if the wind field is intended to be used for fine-scale analysis of pollution patterns or fire spread, or to larger spacing if broad geographic coverage is required. Grid spacing of 500 m is probably the minimum the model will treat properly. Close grid spacing does not permit a 50- by 50-point grid to include major terrain features. These two nonmodel dependent factors (terrain complexity and computer resources) must be considered in selecting the grid interval. The spacings specified here represent maximum spacing—not optimum for any particular application.

The seven cases in this analysis all came from detailed mesometeorological research studies. Such intensive data would not normally be available. Detailed temperature patterns can be estimated from climatological relationships developed for slope temperatures. Super and Grainger (1969) and Hayes (1941) made detailed studies of slope temperatures by aspect and time of day. Baker (1944), using maximum and minimum temperatures, characterized the slope temperatures for 20 mountainous areas of the Pacific and Rocky Mountain States. These climatological relationships will approximate the temperature distribution when the available observations and topography are used to fine tune the slope functions.

Using the Model for Planning—A Case Study

Consider a case where engineers and architects are designing a new plant at a mine mouth. The mineral extraction process will create a large volume of tailings over a period of years. These tailings could be hot. In the design study the questions are asked: (1) What will be the effect of changing the terrain in the immediate area by filling the gulches and small valleys with tailings on the downwind dispersal of stack contaminants?, and (2) What will be the effect on downwind dispersal if the tailings are approximately 70°C warmer than the surrounding areas?

The wind model may be used to estimate probable consequences of the mining activity on pollution dispersal patterns. To illustrate this use, we assumed a light wind of 0.45 m per second (1 mile per hour) from the southwest; temperature distribution was given by climatology for nighttime conditions. Wind patterns before construction showed well-organized drainage flow into and down the valleys and gulches (fig. 9).

Two cases of land change were simulated to anticipate influence on the local wind patterns. In the first case, the valleys and gulches were filled with heated tailings. Changes in the flow were calculated near the modified landform. Heated areas increased the windspeeds and changed the directions to a uniform south-southwest flow down the major gulch (fig. 10). Airflow in the large river drainage to the north was turned and flowed up canyon. The second case considered was that the same gullies and canyons were filled with tailings, but the tailings were not heated. This modification also increased and organized the drainage flow (fig. 11). Winds were from the southwest over the tailings for this case. How-

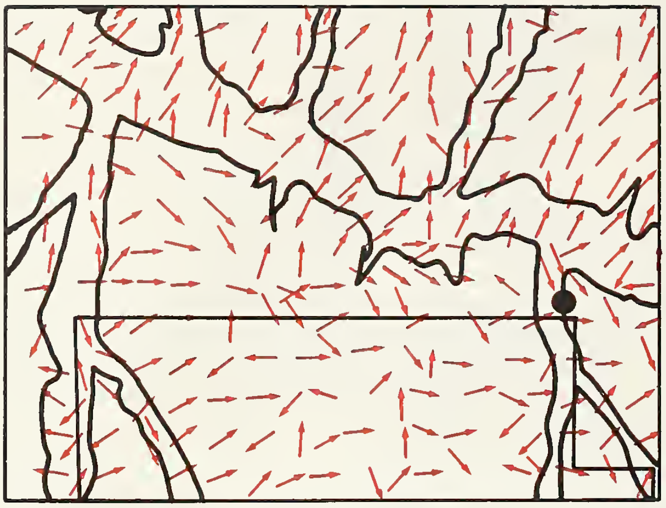

● indicates plant and mine site.

Figure 9.—Local wind pattern before construction of a hypothetical plant and mine tailings.

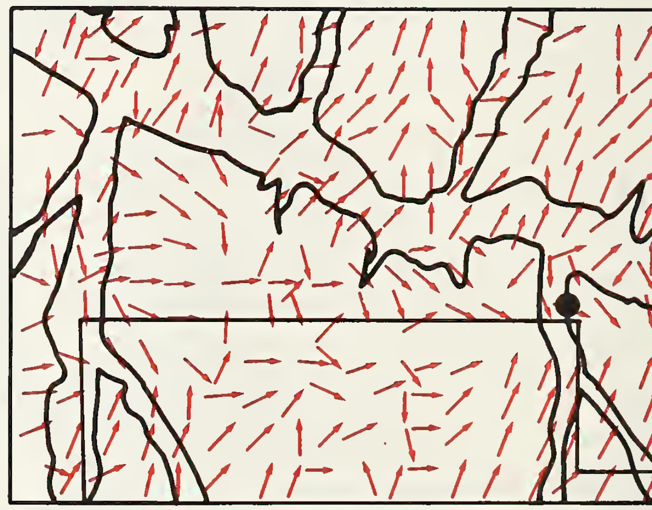

● indicates plant and mine site.

Figure 10.—Simulated wind field for a case with heated tailings.

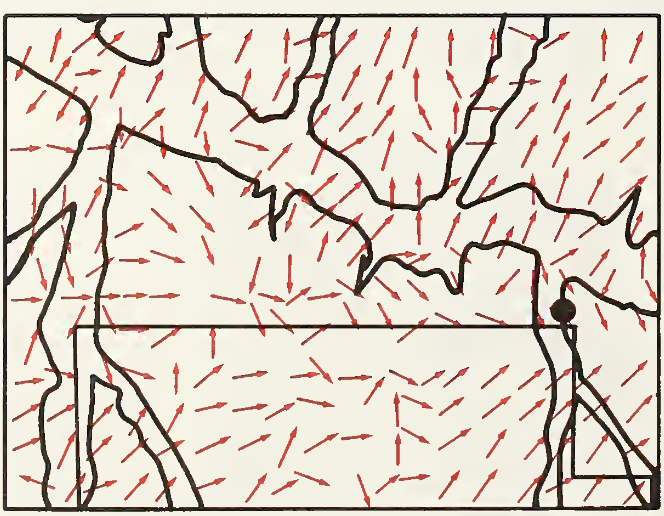

● indicates plant and mine site.

Figure 11.— Simulated wind field for a case with cold tailings.

ever, air did not flow up the canyon from the major river drainage. The two cases predicted increases in windspeed of as much as 1 m per second and direction changes of 180 degrees near the planned mine activities.

Summary and Conclusions

Local thermally driven flows such as mountain and valley winds are simulated reasonably well. Interactions of these local flows, and influence of the larger scale potential flow on these local winds, are also included in the resultant flow. These thermally driven flows are determined properly primarily because the thermal forcing processes are stationary and locked to the terrain features. Also, these thermal features are in a quasi-steady state for several hours. Thus, neglect of the advective process is permissible, and the impulse integration to steady state approximates the flow field.

Thermal modification of potential flow across the terrain features dominates the driving forces. Potential flow was three times as important as rotational flow.

Error analysis of seven case studies and the application example indicated that the model could be used as an aid in fire and air-quality programs because of the low data requirements and the reduced computer effort required.

The wind model developed here was based on simplifications of the complete set of equations governing atmospheric flow over complex terrain. These simplifications imposed several limitations on the use of the model, both in types of flow that can be depicted and in spatial coverage of the solutions. Moving flow systems and flows which are characterized by intermittency or by separation are explicitly excluded, because (1) advection was eliminated, and (2) the model is intended to depict quasi-steady state processes. Coefficients describing static stability and overall wind through-flow place spatial limits on the model because (1) constant static stability prohibits larger scale baroclinicity, and (2) the single-valued wind vector prohibits large-scale flow discontinuity. Also, the neglect of advective processes excludes strong interaction of the mesoscale with larger scales, and does not allow for modification of the downwind environment.

Literature Cited

Anderson, Gerald E.
1971. Mesoscale influences on wind fields. J. Appl. Meteorol. 10:377-386.

Baker, Fredrick S.
1944. Mountain climates of the western United States. Ecol. Monogr. 14:223-258.

Cramer, Owen P.
1972. Potential temperature analysis for mountainous terrain. J. Appl. Meteorol. 11:44-50.

Cramer, Owen P., and Robert E. Lynott.
1961. Cross section analysis in the study of windflow over mountainous terrain. Bull. Am. Meteorol. Soc. 42:693-702.

Cramer, Owen P., and Robert E. Lynott.
1970. Mesoscale analysis of a heat wave in western Oregon. J. Appl. Meteorol. 9:740-759.

Fosberg, Michael A.
1967. Numerical analysis of convective motions over a mountain ridge. J. Appl. Meteorol. 6:889-904.

Fosberg, Michael A.
1969. Airflow over a heated coastal mountain. J. Appl. Meteorol. 8:436-442.

Fosberg, Michael A., and Mark J. Schroeder.
1966. Marine air penetration in central California. J. Appl. Meteorol. 5:573-589.

Fosberg, Michael A., Albert Rango, and William E. Marlatt.
1972. Wind computations from the temperature field in an urban area. Proc. Conf. on Urban Environ. and second Conf. on Biometeorol., Oct. 31-Nov. 2, Philadelphia, Pa. p. 5-7.

Hayes, G. Lloyd.
1941. Influence of altitude and aspect on daily variations in factors of forest fire danger. U.S. Dep. Agric., Circ. 591, 37 p.

Priestley, C. H. B.
1959. Turbulent transfer in the lower atmosphere. 130 p. Univ. Chicago Press.

Sellers, William D.
1965. Physical climatology. 272 p. Univ. Chicago Press.

Super, Arlin B., and Anthony C. Grainger.
1969. Studies of the diurnal wind and temperature regimes above mountain slopes. Dep. Earth Resour., Mont. State Univ., Bozeman, Mont. Final rep. to U.S. Dep. Comm., Environ. Sci. Serv. Admin. 77 p.

Sutton, O. G.
1953. Micrometeorology. 333 p. McGraw-Hill, N.Y.

APPENDIX

List of Symbols

Symbol	Definition	Units
c_p	Specific heat at constant pressure	1.003 joules $gm^{-1}\ {}^oK^{-1}$
f	Coriolis parameter	sec^{-1}
g	Acceleration of gravity	9.8 m sec^{-2}
H	Thickness of rigid lid layer	m
h	Thickness of second approximation to flow	m
k	von Karman constant	0.4
$\underset{\sim}{k}$	Unit vector in vertical direction	dimensionless
K	Turbulent viscosity	$m^2 \cdot sec^{-1}$
p	Pressure	dynes cm^{-2}
p_o	Reference pressure	10^6 dynes cm^{-2}
p_*	Non-dimensional pressure $\left(\frac{p}{p_o}\right)^{\frac{R}{c_p}}$	----------
R	Ideal gas content	0.287 joules $gm^{-1}\ {}^oK^{-1}$
T	Temperature	Deg K
t	Time	Sec
$u, \overline{u}, u_o$	Windspeed in west to east direction	m sec^{-1}
u_*	Friction velocity in west-east direction	m sec^{-1}
$\underset{\sim}{v}$	Horizontal velocity vector	m sec^{-1}
$v, \overline{v}, v_o$	Windspeed in south-north direction	m sec^{-1}
v_*	Friction velocity in south-north direction	m sec^{-1}
w_w	Vertical windspeed	m sec^{-1}
x	Horizontal coordinate in west-east direction	m
y	Horizontal coordinate in south-north direction	m
z	Vertical coordinate	m
z_o	Surface roughness length	m
$\delta, \overline{\delta}$	Horizontal divergence	sec^{-1}
$\zeta, \overline{\zeta}$	Vertical component of vorticity	sec^{-1}
θ	Potential temperature $\theta = \frac{T}{P_*}$	Deg K
ρ	Density of air	kg m^{-3}
σ	Static stability $\sigma = \frac{1}{\theta}\frac{\partial\theta}{\partial z}$	m^{-1}
ϕ	Velocity potential	$m^2\ sec^{-1}$
ψ	Stream function	$m^2\ sec^{-1}$
∇	Horizontal vector gradient operator	m^{-1}
∇^2	Horizontal laplacian operator	m^{-2}
Δ	Horizontal grid spacing	m
Δt_ζ	Impulse time for vorticity	sec
Δt_δ	Impulse time for divergence	sec

Fosberg, Michael A., William E. Marlatt, and Lawrence Krupnak. 1976. Estimating airflow patterns over complex terrain. USDA For. Serv. Res. Pap. RM-162, 16 p. Rocky Mt. For. and Range Exp. Stn., Fort Collins, Colo. 80521.

A simple one-layer model of atmospheric boundary layer flow was developed for use in complex terrain. The model was derived through simplification of the fundamental Navier-Stokes flow equations.

Although the equations do not describe all flow characteristics, the resultant solution describes a diagnostic model of the vector flow field. It requires much less data than traditional approaches,

The intended primary uses for this model are in providing wind fields for fire behavior prediction and in evaluation of pollution transport patterns.

Keywords: Wind, boundary layer, air pollution, fire weather.

Fosberg, Michael A., William E. Marlatt, and Lawrence Krupnak. 1976. Estimating airflow patterns over complex terrain. USDA For. Serv. Res. Pap. RM-162, 16 p. Rocky Mt. For. and Range Exp. Stn., Fort Collins, Colo. 80521.

A simple one-layer model of atmospheric boundary layer flow was developed for use in complex terrain. The model was derived through simplification of the fundamental Navier-Stokes flow equations.

Although the equations do not describe all flow characteristics, the resultant solution describes a diagnostic model of the vector flow field. It requires much less data than traditional approaches,

The intended primary uses for this model are in providing wind fields for fire behavior prediction and in evaluation of pollution transport patterns.

Keywords: Wind, boundary layer, air pollution, fire weather.

Fosberg, Michael A., William E. Marlatt, and Lawrence Krupnak. 1976. Estimating airflow patterns over complex terrain. USDA For. Serv. Res. Pap. RM-162, 16 p. Rocky Mt. For. and Range Exp. Stn., Fort Collins, Colo. 80521.

A simple one-layer model of atmospheric boundary layer flow was developed for use in complex terrain. The model was derived through simplification of the fundamental Navier-Stokes flow equations.

Although the equations do not describe all flow characteristics, the resultant solution describes a diagnostic model of the vector flow field. It requires much less data than traditional approaches,

The intended primary uses for this model are in providing wind fields for fire behavior prediction and in evaluation of pollution transport patterns.

Keywords: Wind, boundary layer, air pollution, fire weather.

Fosberg, Michael A., William E. Marlatt, and Lawrence Krupnak. 1976. Estimating airflow patterns over complex terrain. USDA For. Serv. Res. Pap. RM-162, 16 p. Rocky Mt. For. and Range Exp. Stn., Fort Collins, Colo. 80521.

A simple one-layer model of atmospheric boundary layer flow was developed for use in complex terrain. The model was derived through simplification of the fundamental Navier-Stokes flow equations.

Although the equations do not describe all flow characteristics, the resultant solution describes a diagnostic model of the vector flow field. It requires much less data than traditional approaches,

The intended primary uses for this model are in providing wind fields for fire behavior prediction and in evaluation of pollution transport patterns.

Keywords: Wind, boundary layer, air pollution, fire weather.

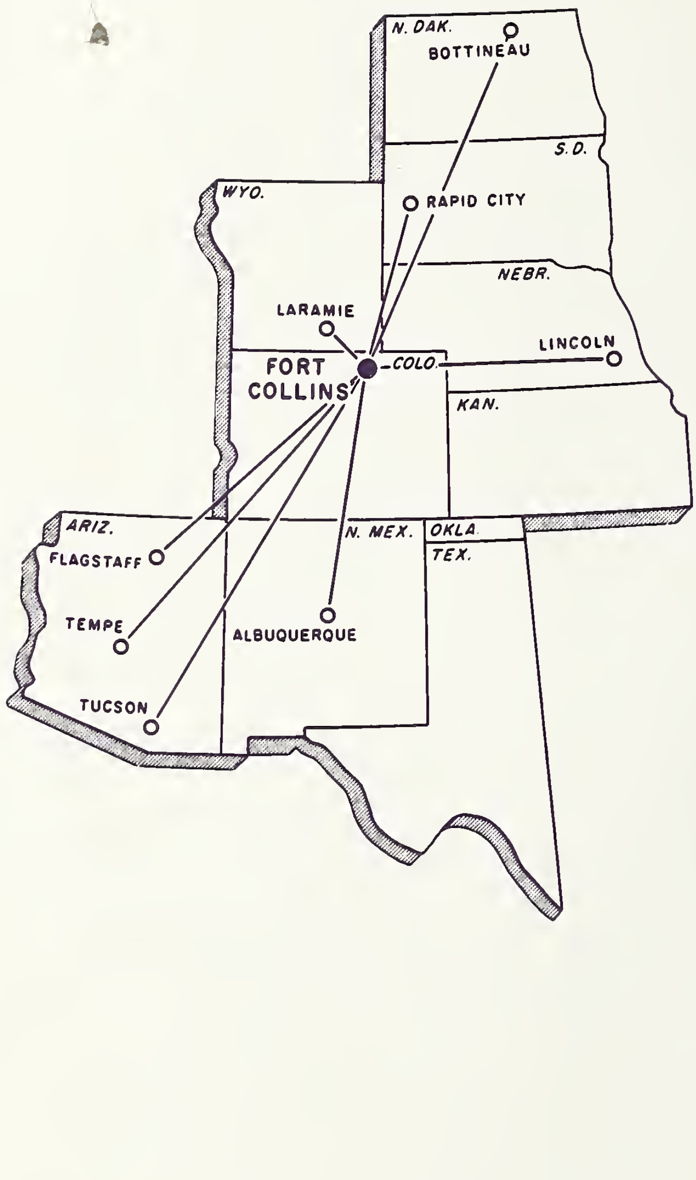
N. DAK.
BOTTINEAU
S. D.
RAPID CITY
WYO.
NEBR.
LARAMIE
LINCOLN
FORT COLLINS
COLO.
KAN.
ARIZ.
N. MEX.
OKLA.
TEX.
FLAGSTAFF
TEMPE
ALBUQUERQUE
TUCSON